4

Propagation of high power parabolic pulses in dispersion oscillating fiber

4.1 Introduction

Formation of parabolic pulses with their characteristic linear frequency chirp has been widely studied and investigated in normally-dispersive fiber amplifiers as well as in passive optical fibers. Such pulses are known to exhibit robust propagation dynamics against strong nonlinearity and the detrimental effect of optical wave breaking. However, it has also been observed that a very high nonlinearity and dispersion induces an excessive amount of phase accumulation leading to an intermediate transient state of propagation rather than forming an asymptotic solution of pulse propagation. In that case, the formed parabolic pulses easily loses their self-similar behavior and results in pulse distortion within a short distance of propagation. In the previous chapter, an input pulse customization technique has been adapted to go beyond the intermediate state of propagation. The presence of the dark pulse in the background of the bright pulse has redistributed the pulse energy in a way to minimize the nonlinear effect, and thus the nonlinear pulse reshaping has occurred at a length beyond the OWB length for the fiber. This technique has been plausible for applications that require fiber based transmission of light through kilometer long distances. However, for short reach (<100 m) robust transmission of high power ultrashort pulse, it becomes eventually difficult to avoid the transient state of propagation as the comparatively high intensity of the propagating pulse will trigger faster reshaping owing to the effect of SPM. Moreover, formation of such parabolic pulses through nonlinear pulse reshaping technique becomes more challenging in a highly dispersive and highly nonlinear environment which essentially occurs during pulse propagation in the mid-infrared range of wavelength (2 to 25 μm). Use of glass materials like chalcogenides are essential for operating in the mid-infrared wavelength range as it exhibits excellent transmission properties in such longer wavelength range where silica or other lead-based soft glasses have higher absorption loss [Sanghera and Aggarwal, 1999; Eggleton et al., 2011]. However, chalcogenide glasses are known to be highly nonlinear, and dispersive so that it may deteriorate and limit the pulse propagation. Thus, formation of parabolic pulses in longer wavelength range demands certain novel technique in terms of fiber engineering to manage such higher dispersion and nonlinearity involved in the state-of-the-art facilities to achieve a stable self-similar propagation. Lately, a lot of research has involved study of various specialty fiber designs for purposes like pulse reshaping, continuum generation, ultra-short pulse delivery, and high-power fiber lasing, etc. For this, a few novel schemes such as fibers with comb-like dispersion profile [Kibler et al., 2006; yu Jiang et al., 2013], trench-assisted large mode area fiber [Sahu and Jain, 2016], dispersion decreasing fiber [Hirooka and Nakazawa, 2004], nonlinearity increasing fiber [Ghosh et al., 2019], and dispersion managed fibers [Finot, 2008] are some of the customized techniques that have been reported in the literature. Precisely, the dispersion managed fibers exhibit great potential towards achieving the self-similar behavior of parabolic pulses preceding the OWB regime which has been retained in presence of both the normal and the anomalous dispersion regime. However, such varying dispersion profile has few variants in its customization which, in turn, reveals new features of pulse propagation through such fibers.

In this chapter, the self-similar propagation of high power ultrashort optical pulses and a rigorous analysis of their stability in various adverse situations have been demonstrated through a specially designed dispersion oscillating Bragg fiber (DOBF). In section 4.2, the design and modal analysis of a chalcogenide glass based Bragg fiber cross-section along with the formation of parabolic pulses in the mid-IR wavelength range has been presented. Moreover, a fiber engineering scheme based on a rapidly varying dispersion profile with near-zero positive GVD has been proposed to stabilize the formed parabolic pulses inside the fiber. Also, propagation of the formed parabolic pulses has been presented through the DOBF. In section 4.3, the propagation dynamics of parabolic pulses with very high repetition rate and their limitations in such dispersion and nonlinearity tailored fiber has been discussed. In section 4.4, the effect of higher order nonlinearity on the propagation of high power parabolic pulses through the designed DOBF has been presented. Moreover, the spectral behavior of the formed parabolic pulses in the DOBF has been analysed and compared to that obtained from a dispersion decreasing fiber. In section 4.5, the effect of higher order dispersion (presence of TOD) on the propagation of parabolic pulses through the designed DOBF has been studied. Further, to reduce the adverse effect of TOD in such DOBF, a transverse chirping mechanism has been implemented along with the longitudinally varying dispersion oscillating profile to achieve stable self-similar delivery of parabolic pulses. Moreover, to appreciate the effect of two-fold fiber engineering on the self-similar pulse evolution, the specialty fiber design and pulse propagation has also been demonstrated in the near-infrared wavelength range.

4.2 Dispersion oscillating fiber

The passive nonlinear reshaping of high power ultrashort optical pulses preceding the wave breaking regime in the mid-infrared range of wavelength essentially becomes unstable due to excessive dispersive as well as nonlinear phase accumulation. Precisely, the high nonlinearity contributes to rapidly generate new frequencies at the pulse edges, and in presence of large amount of normal GVD the chirp becomes non-monotonic owing to the unwanted overlap between the shifted and unshifted frequency components of the pulse. Thus, within a very short range of propagation, the formed parabolic pulses get distorted and take a rectangular shape with oscillations at the pulse edges. Here, the aim is to compensate the excessive dispersive phase accumulation which has been the major factor for the occurrence of the transient response. For this, a novel fiber design scheme based on the rapidly varying dispersion profile with an average normal GVD close to zero has been proposed. It has earlier been reported that parabolic pulses exhibit self-similar evolution also in presence of anomalous GVD [Finot, 2008]. On the basis of this fact, a specialty photonic bandgap fiber with a Bragg cross-section has been designed, whose dispersion profile has been unconventionally tailored for attainment of self-similarity in a highly dispersive and nonlinear medium.

The scheme, to achieve stable self-similar propagation, is endowed with a rapid variation of dispersion and nonlinearity over the propagation length. The designed fiber has two segments based on their specific functions. The initial segment is a dispersion decreasing Bragg fiber to form the parabolic pulses in a short propagation distance. The other segment has been designed to stabilize the formed parabolic pulses which comprises of alternately spliced down-tapered and up-tapered short fiber sections to obtain a varying dispersion profile. Specifically, the dispersion varies rapidly along the fiber length from normal to anomalous dispersion regime globally providing a small positive mean GVD value, while the fiber nonlinearity correspondingly gets simultaneously modulated due to its z-dependence. The fiber has been designed to operate at 2.8 μm wavelength. The availability of laser source at 2.8 μm has driven us to design a parabolic pulse source at this mid-IR wavelength [Wei et al., 2012]. Furthermore, fabrication-compatible chalcogenide glasses at mid-IR have been chosen for a practical design and simulation.

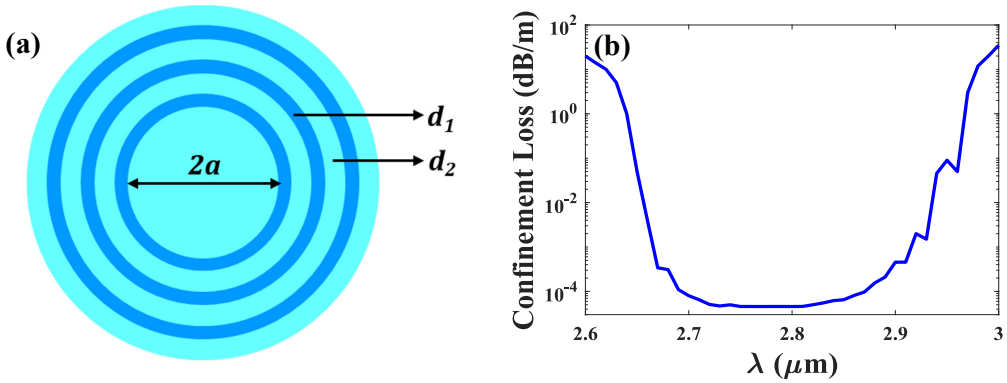

Figure 4.1: (a) The schematic of the Bragg fiber cross-section designed at 2.8 μm, (b) the confinement loss spectrum of the fundamental mode in the designed Bragg cross-section as obtained from the modal analysis using TMM.

4.2.1 Design and modal analysis of the Bragg fiber: Fiber I

To form the parabolic pulse, a Bragg fiber cross-section has been optimized at 2.8 μm. To achieve this, two chalcogenide glasses with slightly different refractive indices but having similar transmission properties at the operating wavelength have been chosen. The thermal conductivity of the two glasses are such that the generated heat would easily be dissipated through the cladding structure. Moreover, other physical parameters of the two materials are in good agreement to have better thermo-mechanical compatibility [Kubat et al., 2014]. The optimization of the thicknesses of high and low index layers are performed by solving the dispersion relation given in equation (1.48) in a MATLAB® code built in-house. Moreover, using equations (1.49) and (1.50), an iterative process has been carried out to obtain an optimized bilayer thickness and the core radius for which the effective refractive index n_{eff} for the fundamental mode remains almost same. Following this procedure, the optimized dimensions are obtained as: core radius $a = 4.5$ μm, high index layer thickness $d_1 = 0.695$ μm, and low index layer thickness $d_2 = 2.94$ μm. Also, three successive bilayers of cladding have been considered surrounding the low-index core. This designed Bragg cross-section has been denoted as Fiber I, and is shown in figure 4.1(a). The modal analysis of this geometry has been done by using TMM as described in section 3.2.1, and the confinement loss spectrum for the fundamental mode has been depicted in figure 4.1(b). The Bragg cross-section has been optimized in a way that the fundamental mode exhibits the tight confinement compared to other higher order modes resulting in their faster decay and effectively single-mode operation of the fiber. The confinement loss of the fundamental mode at 2.8 μm has been estimated to be 4.8×10^{-2} dB/km. It is to mention here that the nonlinear refractive index n_2 of the core material is very high, $\sim 5.2\times10^{-18}$ m^{-2}/W at 2.8 μm. As obtained from the modal analysis of Fiber I, the value of GVD parameter β_2 has been 1.8×10^{-1} ps^2m^{-1} and nonlinear parameter γ has been 3.8×10^{-2} $W^{-1}m^{-1}$, both estimated at 2.8 μm.

Further, with the estimated fiber dimensions and other parameters taken as initial, Fiber I is assumed to be down-tapered with a taper-ratio 0.81 over a length of 2 m to achieve the longitudinally decreasing dispersion profile. Notably, the taper-ratio in this fiber design has been defined as the ratio of the initial to final cross-section considering a linear scaling over fiber length. If the ratio is greater than unity then it is called up-tapered, and for less than unity it is called down-tapered. For Bragg fiber cross-section, a down-tapering is required to achieve a dispersion decreasing profile. The schematic of the down-tapered fiber has been shown in figure 4.2(a), and the corresponding β_2 and γ variation over the fiber length has been depicted in figures 4.2(b) and (c), respectively. The values of β_2 and γ at various fiber cross-sections of the tapered fiber has been

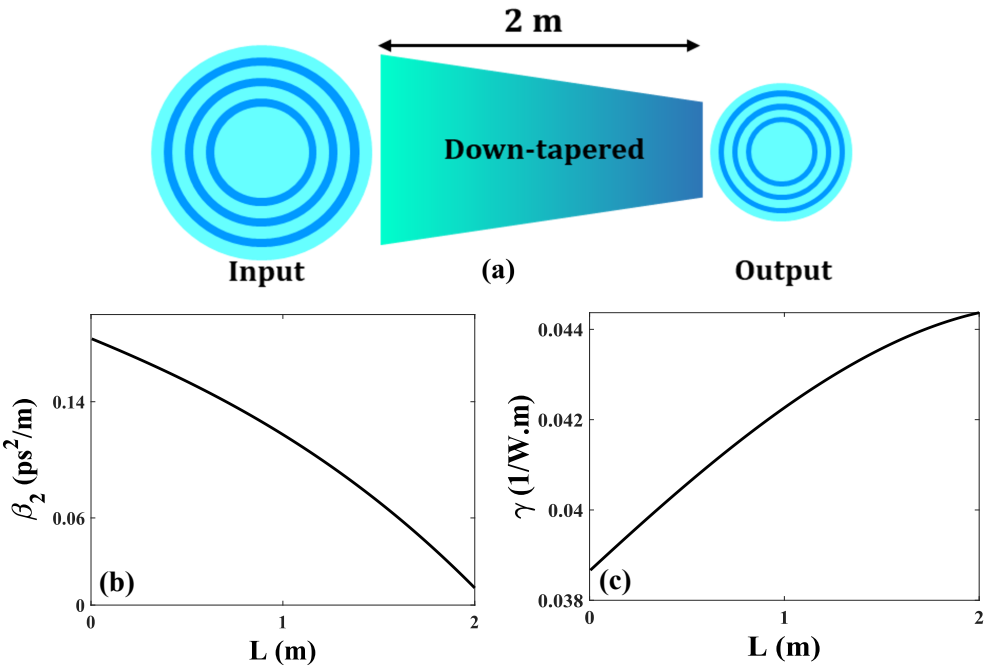

Figure 4.2: (a) The schematic of Fiber I which is a 2 m long down-tapered segment with input and output cross-sections. The corresponding longitudinal profiles of (b) GVD parameter β_2, and (c) nonlinear parameter γ.

estimated from the modal analysis, and has been interpolated to obtain the complete profile. The output end cross-sectional parameters of Fiber I have been (i.e., at 2 m): core-radius $a = 3.64$ μm, $d_1 = 0.56$ μm, $d_2 = 2.38$ μm, $\beta_2 = 1.26\times10^{-2}$ ps^2m^{-1}, and $\gamma = 4.43\times10^{-2}$ $W^{-1}m^{-1}$.

4.2.2 Bragg fiber segment for self-similar parabolic pulses: Fiber II

The other fiber segment having the rapidly varying dispersion profile has been denoted as Fiber II and specifically designed for stable parabolic pulse propagation. The materials of the fiber has been kept same as mentioned for Fiber I. Also, the input-end cross-section of Fiber II has been chosen to be identical to the output-end cross-section of Fiber I as stated in the previous subsection in order to avoid losses due to misalignment. Further, with such initial cross-section, Fiber II has been down-tapered with a taper-ratio of 0.98 over 1 m, so that the value of β_2 starts from a positive GVD value, crosses zero dispersion, and reaches a negative GVD value. This specific dispersion profile of Fiber II on alternate repetition provide a varying dispersion landscape with a nearly mean-zero β_2 value with a positive sign. Such a dispersion tailoring in Fiber II has been deliberately exploited in order to customize the global dispersive effect of fiber on pulse propagation, along with associated modulation in γ, so as to achieve self-similarity of the formed parabolic pulses. The schematic representation of the total Fiber II segment has been shown in figure 4.3(a). Moreover, the longitudinal variations of β_2 and γ are depicted in figures 4.3(b) and (c), respectively. Here also, the longitudinally varying curves have been obtained by estimating the values of $\beta_2$and γ at various cross-sections of the 1 m long tapered section.

The entire dispersion profile of the proposed segmented fiber with both Fiber I and Fiber II connected together following the proposed scheme has been illustrated in figure 4.4(a). Corresponding, variation of γ has been shown in figure 4.4(b) for the segmented DOBF over an arbitrarily chosen length of 8 m. The average value of β_2 during propagation through Fiber II is 5.5×10^{-3}

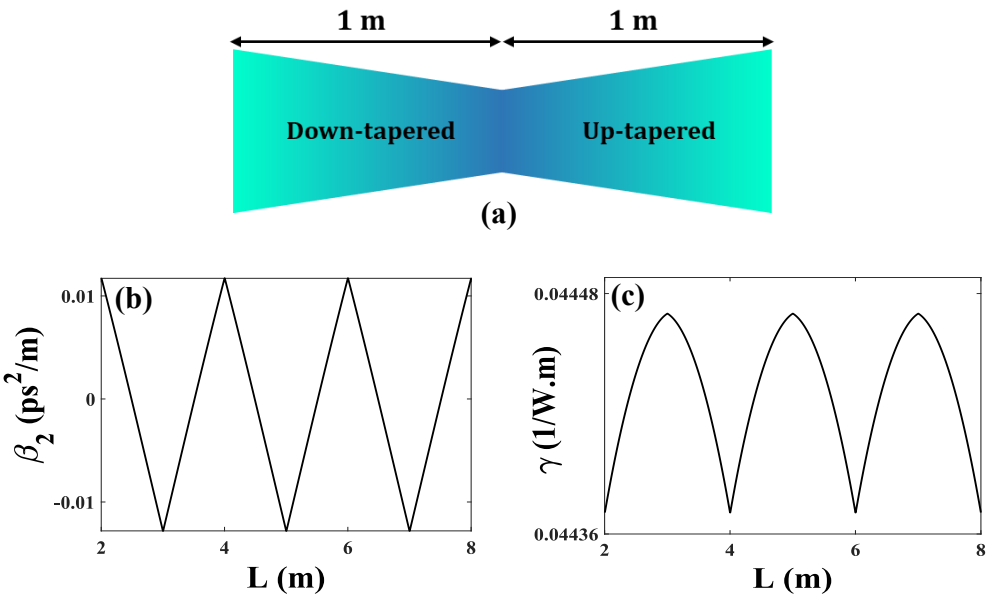

Figure 4.3: (a) The schematic illustration of the Fiber II clubbing a 1 m long down-tapered section with a 1 m long up-tapered section to achieve oscillating dispersion profile. The corresponding longitudinal profiles of (b) GVD parameter β_2, and (c) nonlinear parameter γ over 6 m long Fiber II segment.

ps^2.km^{-1}, which is nearly same or fixed for each fiber segment as the segments have been identical to itself and varied linearly; also the nonlinearity due to SPM has an average value given by, $\gamma =$ 44 W^{-1}.km^{-1}. It is to mention here that the proposed oscillating dispersion variation along with nonlinearity modulation over length could be otherwise achieved by a single fiber with simultaneous up-and-down tapering. However, fabrication of such structures using chalcogenide glasses via state-of-the-art fabrication processes may be somewhat challenging. Hence from the view-point of easier fabrication, the segmented fiber consisting of a 1 m long sections with zero-crossing longitudinal dispersion profile has been demonstrated that can be spliced with another identical fiber tapered reversely and the process could be continued over longer distances with some compromise in loss penalty.

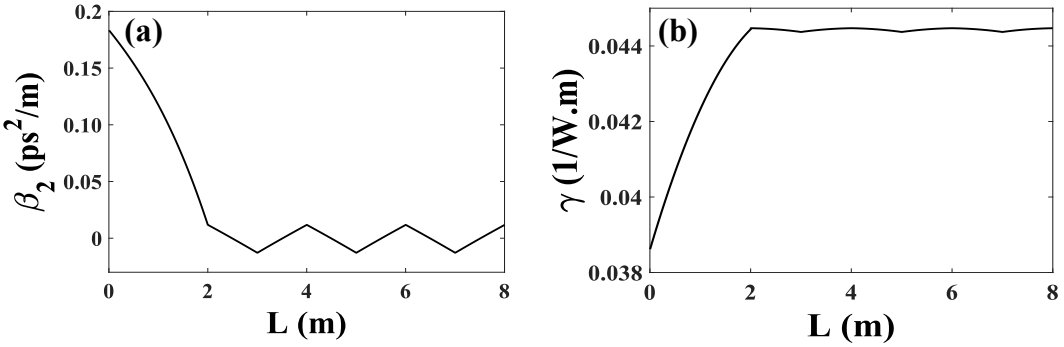

Figure 4.4: The longitudinal variations of (a) GVD parameter β_2, and (b) nonlinear parameter γ over 8 m long designed DOBF.

4.2.3 Propagation of Parabolic pulses in DOBF

In order to study the formation and propagation of parabolic pulses through the designed 8 m long DOBF, a slowly varying pulse envelope A(z, T) of a standard Gaussian pulse have been chosen as the input pulse form, and its evolution dynamics through the designed DOBF has been studied by numerically solving NLS equation of the form,

$$\frac{\partial A}{\partial z} - i\frac{\alpha}{2}A + i\frac{\beta_2(z)}{2}\frac{\partial^2 A}{\partial T^2} - i\gamma(z)|A|^2 A = 0, \tag{4.1}$$

where, $\beta_2(z)$ and $\gamma(z)$ are the length dependent GVD and nonlinear parameters as estimated at various lengths of the tapered sections. The NLS equation has been solved numerically implementing SSFM in a MATLAB® code developed in-house. It is to mention that the variation in the loss parameter α over the entire fiber length has been assumed to be constant, as the contribution of the confinement loss (which should be varying with the tapering) to the total optical loss has been negligible. Since the DOBF has several sections to be spliced, thus we have considered the splice loss along with the material and the confinement loss of the fiber. Considering the nearly perfect cross-sectional geometries and mode-field diameters of the fiber segments, the extrinsic loss accumulated per splice has been 0.08 dB/m, confinement loss 4.8×10^{-5} dB/m, and material loss for the core material has been taken to be 0.2 dB/m.

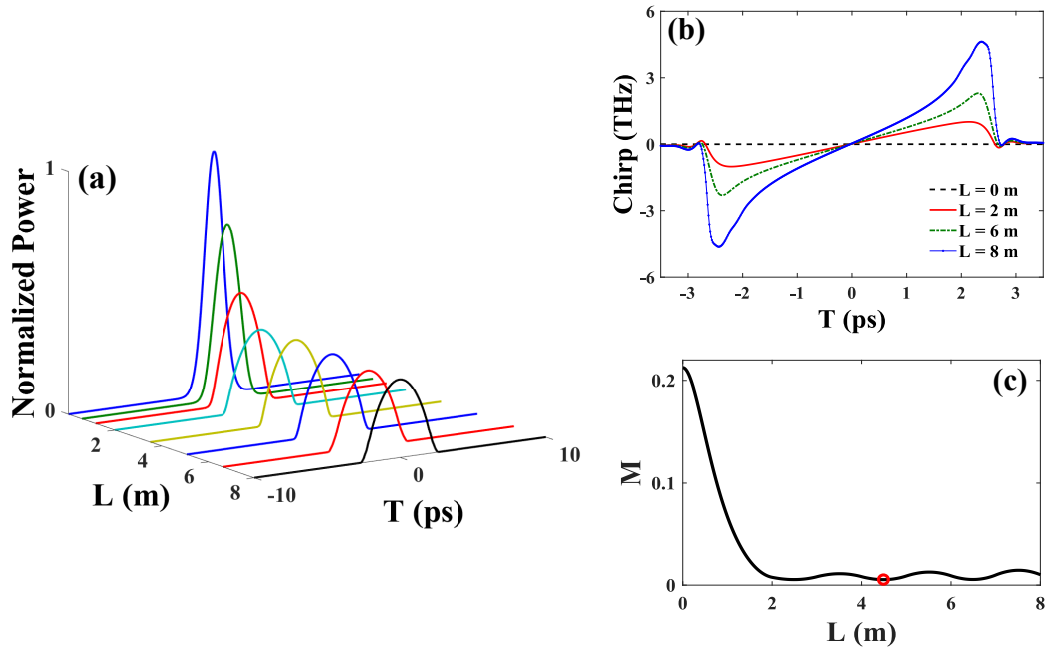

Figure 4.5: (a) The formation of parabolic pulse from an input Gaussian pulse, (b) the corresponding frequency chirp across the pulse width at various fiber lengths, and (c) the variation of misfit parameter M through the 8 m long chalcogenide glass based DOBF at 2.8 μm.

The evolution of an unchirped Gaussian pulse of peak power 150 W and full-width-at-half-maximum (FWHM) 2.0 ps centered at 2.8 μm has been observed through the 8 m long designed DOBF. The evolution of the input pulse is depicted in figure 4.5(a). We can observe that within 2 m length of the fiber, the Gaussian profile is reshaped into a parabolic one, and has shown a stable self-similar evolution through the rest part of the fiber. The stable evolution dynamics has indeed demonstrated that the dispersion oscillating landscape does provide significant reduction in the dispersive phase accumulation and thus results in self-similar pulse propagation even in such a highly nonlinear and dispersive environment. It is interesting to note that the propagation of parabolic pulses through the dispersion oscillating fiber segment exhibits a very little amount of

broadening and the pulse shape remains almost identical as it has been at the end of Fiber I segment. This kind of evolution can be generally observed in case of a very small dispersive effects, and is very interesting from the application point of view where dispersion-induced broadening is totally undesired. In figure 4.5(b), the evolution of the frequency chirp at various propagation length has been shown. It can clearly be seen that the chirp is linear across the entire width of the formed parabolic pulse which holds the importance of such pulses being robust against strong nonlinearity. However, it can also be observed that at the pulse edges the chirp variation has become steeper which may indicate a gradual distortion on further propagation due to strong nonlinearity. Figure 4.5(c) depicts the evolution of the misfit parameter M estimated by using the expression given in equation (3.18) over the entire DOBF length. The evolution explicitly indicates the self-similar behavior of the parabolic pulse which has reached a minimum misfit value of ∼0.019 as denoted by the red circle, and has been maintained across such a lower misfit value throughout the rest of the fiber length. Moreover, the misfit parameter evolution strictly dictates that the formed parabolic pulses have surmounted any significant dispersion-induced broadening owing to the globally experienced close-to-zero average GVD value of the Fiber II segment.

4.3 Quasi-CW propagation of parabolic pulses in DOBF

In this section, the stability of the formed parabolic pulses through the designed DOBF at 2.8 μm with a high pulse repetition rate has been investigated. To study the dynamics of pulse propagation with high pulse repetition rate, Gaussian seed pulses with peak power 90 W and 1.5 ps of FWHM are fed at the input end of the DOBF. The pulse propagation has been studied by numerically solving equation (4.1). Initially, two identical Gaussian inputs at the repetition rate of ∼167 GHz have been considered. After propagating through the initial 2 m of the total fiber length, parabolic pulses with linear chirp across its width have been achieved, which further propagates through the rest of the fiber length unperturbed maintaining its parabolic temporal profile intact. The stable quasi-CW propagation of the parabolic pulses has been shown in figure 4.6(a), whereas figure 4.6(b) depicts the variation of chirp across the pulse width. It can clearly be observed that the consecutive two Gaussian inputs, separated by 6 ps in time scale, are now converted into two distinct parabolic pulses without any kind of overlap or distortion. Each of the distinct linear frequency chirp developed within the respective pulse duration has established the stability of the formed parabolic pulses. Hence we claim that the oscillating dispersion and nonlinear profile has supported stable formation of successive parabolic pulses.

To appreciate this aspect of parabolic pulse formation, three consecutive Gaussian pulses with the previous specifications has been launched at the input end of the fiber. Figure 4.6(c) depicts the stable and self-similar evolution of parabolic pulses over the entire 8 m fiber length. Here also, one can explicitly observe the unperturbed transmission of the three closely propagating pulses. It can be concluded that the reduced dispersive effect due to the presence of the dispersion oscillating segment has led to a negligible amount of dispersion induced pulse broadening, and thus their stable transmission without any overlap has been possible. Moreover, figures 4.6(d) and (e) show the chirp variation and spectral evolution of the formed parabolic pulses along different fiber lengths. Interesting has been the spectral evolution which exhibits a comb-like spectral profile, precisely symmetric around the central wavelength. The frequency combs have been found to be nearly equally-spaced, but with varying intensity. Hence, with further scaling of input pulse repetition rate and analyzing the parametric dependence, one can realize the formation of quasi-CW parabolic pulses along with spectral combs from any standard input shape of conventional sources. It is to mention here that input pulses with much shorter pulse width can be transmitted self-similarly through the DOBF, however at a lower pulse repetition rate. Such quasi-CW propagation of parabolic pulses would be interesting for high power delivery and supercontinuum generation

in mid-infrared wavelength range. A judicious choice of mid-infrared glass which exhibits good transparency and lower nonlinearity would be able to deliver near-CW high peak power pulses for the aforementioned applications.

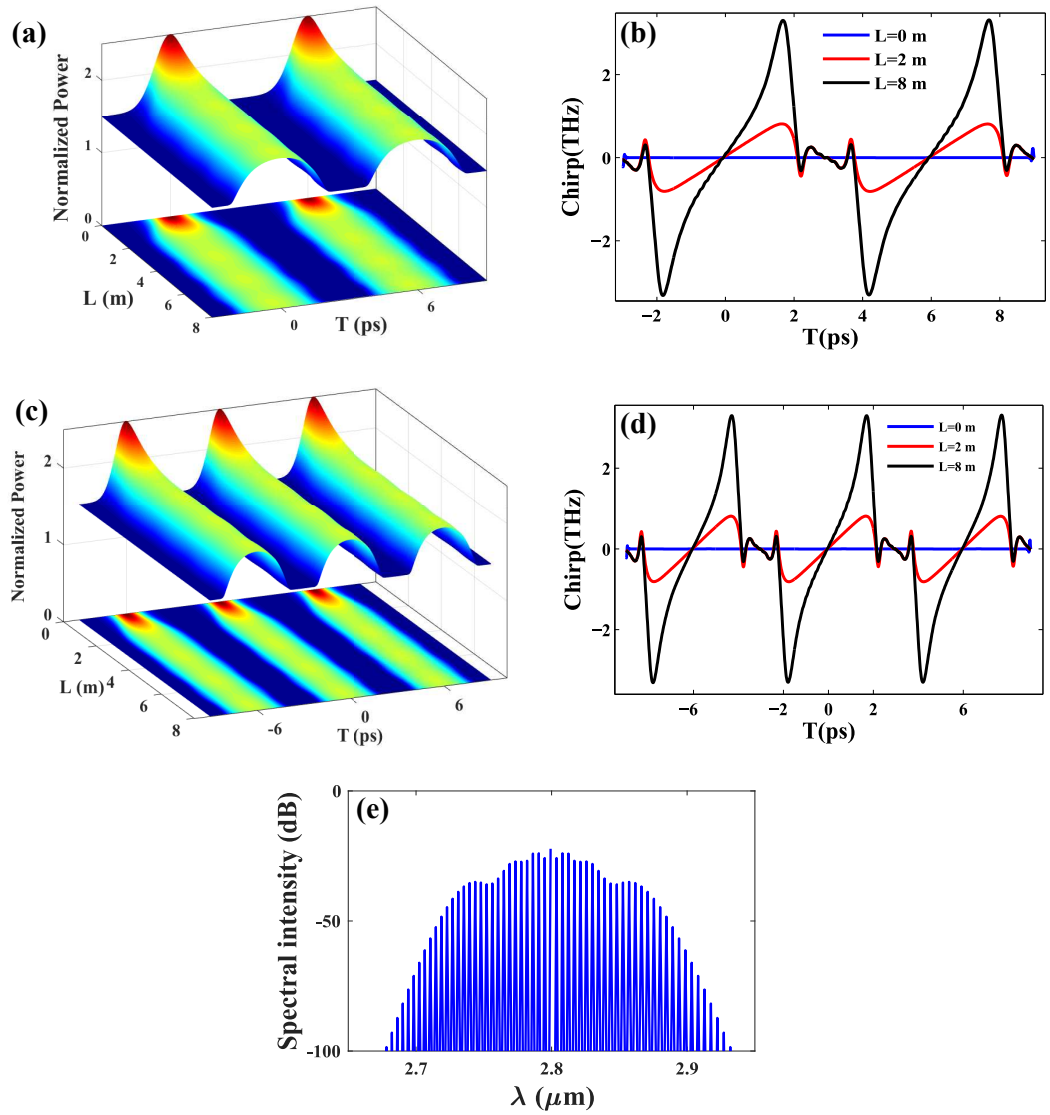

Figure 4.6: The evolution of (a) two consecutive input Gaussian pulses into output parabolic pulses, and (b) the corresponding frequency chirps across their pulse width through the DOBF; the evolution of (c) three consecutive input Gaussian pulses into output parabolic pulses, and (d) their corresponding frequency chirp through the DOBF; (e) the comb-like output spectrum at the end of the DOBF for three consecutive pulses.

4.4 Spectral response on inclusion of higher order nonlinearity

In this section, the possibilities and limitations of the formation of a continuous spectrum along with a smooth temporal parabolic pulse at the end of the designed DOBF has been demonstrated in the presence of higher order nonlinear effect. Recently, generation of pulse-preserving wide continuum in all-normal dispersive fibers were touted for potential applications in time-resolved spectroscopic measurements that essentially demand a flat spectrum over a broad wavelength range [Bassi et al., 2004; Wojtkiewicz et al., 2019]. Such time-resolved measurements are very useful

to understand the dynamics of various chemical processes that occur on time scales of picosecond to femtosecond. Time-resolved infrared spectroscopy, time-resolved fluorescence spectroscopy are such methods, which largely employ the technique to obtain the structural information as well as kinetics of the process. Moreover, such single-pulsed continuum light could also be exploited to obtain few-cycle pulses, and amplified supercontinuum in various parametric processes.

The aim is to investigate the generation of a wide spectrum from a picosecond input pulse while maintaining a smooth temporal parabolic output through a fiber considering up to second order dispersion terms, Kerr type nonlinearity, two-photon absorption, and intrapulse Raman Effect. For this, a standard unchirped Gaussian pulse of peak power 200 W, and FWHM 1.5 ps has been chosen to launch at the input end of the designed DOBF. The pulse parameters have been optimized after several numerical iterations of the pulse propagation equation of the form,

$$\frac{\partial A}{\partial z} + \frac{\alpha}{2}A + i\frac{\beta_2}{2}\frac{\partial^2 A}{\partial T^2} = i\left(\gamma + i\frac{\alpha_2}{2A_{eff}}\right)\left(1 + \frac{i}{\omega_0}\frac{\partial}{\partial T}\right)A\int_{-\infty}^{\infty} R(t)|A(z,t)|^2 dt, \tag{4.2}$$

over a range of power (from few Watts to several kilowatts) and width (picosecond range) on the basis of obtaining maximum spectral broadening with best fitted parabolic pulse at the output end of the fiber. The various fiber parameters in equation (4.2) such as loss parameter α, GVD parameter β_2 and nonlinear parameter γ has been same as stated in section 4.2. Further, in equation (4.2), the nonlinear response function that takes in to account the process of intrapulse Raman scattering has been estimated by the conventional relation,

$$R(t) = (1 - f_R)\delta t + f_R h_R(t) \tag{4.3}$$

where, f_R represents the fractional contribution of the delayed Raman response to nonlinear polarization and $h_R(t)$ is the Raman response function given by equation (2.57). The other nonlinear parameters taken for simulation are as follows: TPA coefficient $\alpha_2 = 9.3 \times$ 10-14 m.W^{-1}, fractional nonlinear contribution $f_R = 0.148$, for calculation of Raman response function $\tau_1 = 23.1$ fs, and $\tau_2 = 195.0$ fs, all for the core material at 2.8 μm.

Evolution of the spectrum has been depicted in figure 4.7(a). Starting from the initial Gaussian spectral profile, the spectrum has gradually broadened due to the modulated high nonlinearity of the fiber. One can observe that at 2 m of the fiber length from the input, it is broadened by only 160 nm with a flat and narrow top. Further propagation through DOBF broadens the spectrum up to ∼465 nm at 20dB points covering a wavelength range from 2.58 µm to 3.05 µm. Moreover, the shape of the spectrum is nearly parabolic with two large kinks at its edges and some small ripples towards the center. Such ripples at the top of the spectrum may be due to the periodic nonlinear modulations and mainly dominated by SPM. However, the broadening of the spectrum has been due to the presence of both the SPM and the intrapulse Raman Effect. Here, it is to be noted that the spectral broadening is restricted to several hundred nanometers, unlike conventional supercontinuum generation. One possibility of such limitation could be that the phase accumulated due to the linear GVD and higher order nonlinearity are being canceled out, which suppress further generation of new frequencies. Moreover, since the DOBF covers both the dispersion regimes (anomalous and normal), the linear phase accumulation is either very small or being counterbalanced giving rise to suppressed spectral broadening. This can be justified from the reference [Mussot et al., 2018] where the strength of the instability has been described with a longitudinally varying dispersion profile either entirely in the normal regime or in the anomalous regime. They also showed that normal GVD leads to better outcomes in terms of spectral broadening. Thus, it has been envisaged that such limitation can be mitigated by judiciously choosing the fiber design parameters.

The corresponding temporal profile of the output pulse has been depicted in figure 4.7(b) along with the evolution of the frequency chirp. One can clearly observe that the input Gaussian

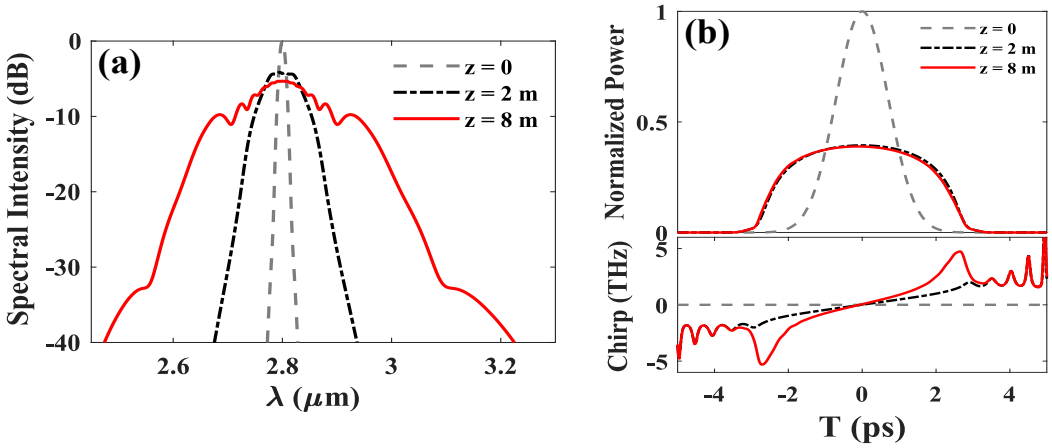

Figure 4.7: (a) The spectral profiles at various lengths of the 8 m long DOBF in presence of higher order nonlinearity, and (b) the corresponding time-domain pulse profiles along with the frequency chirp developed across the pulse width as shown in the lower panel.

pulse has got reshaped to a parabolic profile through the Fiber I counterpart of the DOBF with 4.20 ps output FWHM along with its characteristic linear chirp. The minimum misfit value M^2 is ∼0.0193 at 2 m of the DOBF length. The so formed parabolic pulse further evolves through propagation in Fiber II in a self-similar fashion keeping its power, width, and in turn, its shape intact over rest of the fiber length indicating a breather like propagation dynamics through the DOBF. This is unlike other self-similar pulse propagation reported till date and should be widely applicable for transient absorption spectroscopy, where the measured absorption spectrum of the sample material is a function of both wavelength and time (in the range of few picoseconds to femtoseconds). Moreover, the chirp at the output has been observed to be linear at the end of 2 m, but with further propagation it has developed a sharp deviation at the pulse edges, as observed earlier. It is assumed to be a result of excessive nonlinear phase accumulation.

For better understanding of the findings, the spectral evolution of the same input Gaussian pulse (with 200 W peak power and 1.5 ps FWHM) have been numerically simulated through a normally-dispersive dispersion decreasing Bragg fiber (DDF) vis-à-vis our designed DOBF. The DDF has also been considered to be a Bragg fiber with its initial cross-section identical to that of the input specifications of the DOBF, and to have a gradually decreasing dispersion profile characterized by the equation (3.15) indicating a hyperbolic dispersion profile. For this analysis, $D(0)$ = -44 ps.km^{-1}.nm^{-1} that corresponds to the initial β_2 value of the DOBF, and $\Gamma_0 = 0.028$ as a standard. All other nonlinear fiber parameters have been kept same as for the DOBF. The dispersion variation over fiber length has been depicted in figure 4.8(a). One can easily observe that for the DDF the dispersion values all along the fiber length are much higher in comparison to the average dispersion in the DOBF. In figure 4.8(b), the output spectral densities for both the DDF and the DOBF at various fiber lengths have been plotted. Moreover, figure 4.8(c) clearly depicts that the time-domain output pulse through DDF (solid gray curve) is far away from being a parabolic one with largely spread pulse edges. This is due to the presence of large value of the dispersion that actually broadens the pulse temporally. However, it has maintained a smooth spectral profile as depicted in 4.8(b), although the spectrum has been much narrower than that obtained from its DOBF counterpart. It has only widened up to 128 nm at the 20dB point, whereas output spectrum from DOBF has broadened up to 465 nm, both in the presence of higher order nonlinearities. This observation eventually establishes the advantage and benefit of the dispersion oscillating landscape over a dispersion decreasing one in order to achieve pulse-preserving spectral broadening. The oscillating dispersion landscape was specially designed to provide the pulse a much

smaller average value of dispersion compared to the counterpart DDF so that it experiences much lesser temporal broadening and preserve the pulse shape, which indeed have been reflected in the observations. However, it also limits the order of spectral broadening, which still spans over several hundreds of nanometers.

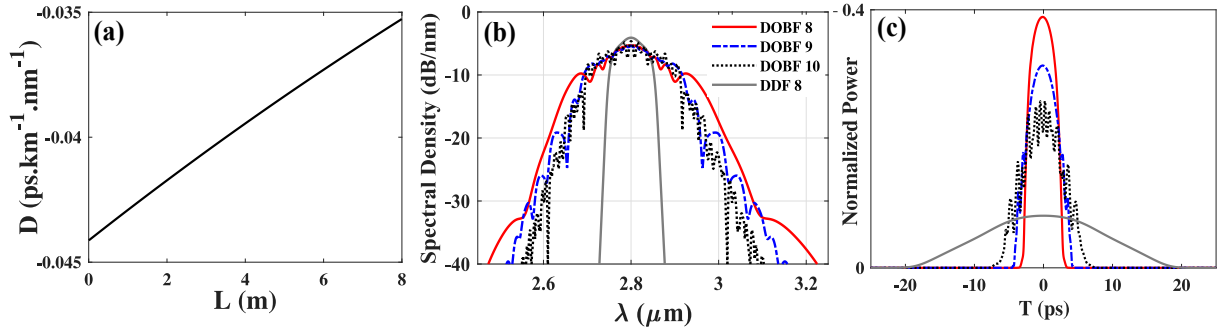

Figure 4.8: (a) The longitudinal dispersion profile of the DDF, (b) the output spectral profiles at various lengths of the DOBF along with the output spectrum obtained at the end of the DDF (gray solid curve), and (c) the corresponding time-domain output pulse profiles.

Furthermore, the evolution of the pulse has been studied by propagating the pulse beyond 8 m of the DOBF length. In figures 4.8(b) and (c), the corresponding temporal and spectral profiles has been shown at the end of 9 m and 10 m of the designed DOBF. The results have explicitly shown that the pulses in time-domain got distorted with further propagation, and the top of the spectra have been observed to be narrowed down further with respect to that obtained at the end of 8 m with increased number of oscillations. It has been assumed that such spectral narrowing beyond a certain length is due to the generation of higher number of new frequencies in the wave-breaking regime. This mechanism results in stronger side lobes in the spectrum with a narrower top. However, this observation is unlike what is reported in [Liu et al., 2012], where the spectral tails appear as side lobes in wave-breaking regime with an extended spectral top.

4.5 Effect of inclusion of higher order dispersion

In the proposed dispersion oscillating Bragg fiber design, the dispersion curve, as shown in figure 4.4(a), has crossed the zero value of the GVD parameter several times, for which the inclusion of the higher order dispersion terms in the pulse propagation equation becomes essential. Precisely, effect of the third order dispersion (TOD) on pulse propagation around the zero dispersion wavelength may become detrimental leading to severe pulse distortion. As previously it has been observed in a dispersion decreasing landscape that if the ratio of the effective length of TOD $L_D^{'}$ to the effective length of GVD L_D is much greater than unity, it limits the stable propagation length of the pulse leading to asymmetric broadening and oscillations in both the temporal and the spectral domains [Latkin et al., 2007; Zhang et al., 2009; Iakushev et al., 2012]. Thus, the impact of TOD on the stable propagation of the parabolic pulses inside the DOBF has been investigated and presented in this section.

To study the pulse propagation through the DOBF in presence of TOD, a slowly varying pulse envelope $A(z,T)$ of Gaussian form has been considered to be the input pulse form, and the pulse propagation has been studied by solving the NLSE of the form,

$$\frac{\partial A}{\partial z} + \frac{\alpha}{2}A + i\frac{\beta_2(z)}{2}\frac{\partial^2 A}{\partial T^2} - \frac{\beta_3(z)}{6}\frac{\partial^3 A}{\partial T^3} = i\gamma(z)|A|^2 A, \tag{4.4}$$

where, $\beta_3(z)$ is the length dependent TOD coefficient, and all other terms have their usual meanings.

As described previously for other fiber parameters in DOBF, the values of β_3 also has been estimated at various fiber lengths from the modal analysis, and has been interpolated to obtain the complete profile as shown in figure 4.9(a). An unchirped Gaussian pulse of peak power 150 W and FWHM 2.0 ps centered at 2.8 μm has been allowed to propagate through the designed DOBF in presence of TOD, where all other fiber parameters have been identical as stated in section 4.2. The temporal and spectral profiles of the pulses at various fiber lengths have been depicted in figures 4.9(b) and (c), respectively. It is explicit from figure 4.9(b) that the formed parabolic pulse has been severely distorted at only 4 m of the fiber length with an asymmetric large oscillation. The similar feature has been observed in 4.9(c) exhibiting a strong distortion of the pulse spectrum along with the asymmetry in the spectral profile. Presence of such asymmetry is the signature of TOD effect, and the large oscillations are due to their large values around the zero dispersion regimes. It is to mention here that there are two factors that amounts to such large TOD values - one is the mandatory use of highly dispersive chalcogenide glasses in the mid-IR wavelength range, and the other one is the large dispersion slope resulted from the down-tapering over small fiber length. In order to mitigate the detrimental TOD effect on the self-similar propagation of the formed parabolic pulses through the DOBF, a two-fold fiber engineering technique has been adapted, and demonstrated in the next subsection.

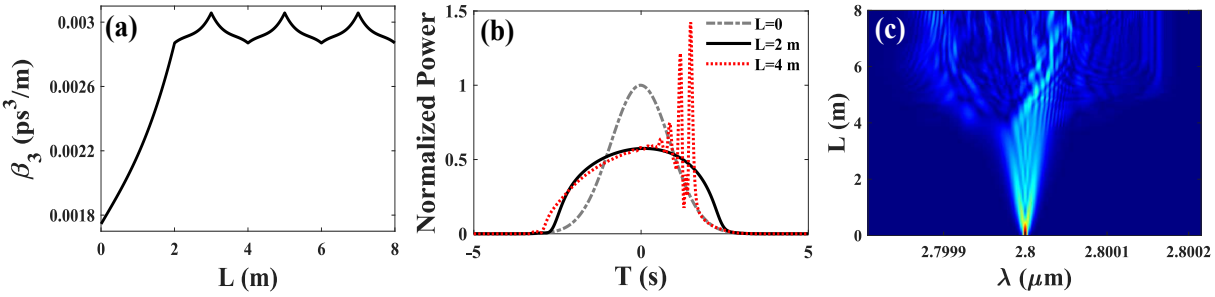

Figure 4.9: (a) The profile of the TOD coefficient β_3 along the 8 m long DOBF, (b) the input and output pulse profiles up to 4 m of the DOBF in presence of TOD, and (c) the corresponding spectral evolution through the total fiber length.

4.5.1 Parabolic pulses in chirped-clad DOBF at mid-IR

Here, the aim is to reduce the effect of TOD in the dispersion oscillating landscape. As it has already been identified that to lower the TOD values, the slope of the GVD curve has to be flattened as much as possible. Such tailoring of the dispersion curve has been possible by implementing a transverse chirping in the Bragg fiber cross-section. In order to implement the two-fold fiber design scheme, a Bragg fiber with an aperiodic cladding structure along with a longitudinally varying dispersion has been proposed. It has been reported earlier that an introduction of transverse chirping in the cladding region is an interesting tool to control the dispersion of the microstructured fibers as well as to eliminate the detrimental effect of TOD [Skibina et al., 2008; Ghosh et al., 2010].

For this chirped-clad fiber design at mid-IR, the same chalcogenide glasses has been considered as previous, and the operating wavelength have been chosen to be 3.0 μm. The fiber design has two segments based on their functioning – Fiber I for parabolic pulse formation, and its counterpart Fiber II for the stable propagation of the formed parabolic pulses. Both Fiber I and Fiber II have 6 bilayers in their cladding which have been linearly chirped from the inner most layer adjacent to the core to the outermost layer. The two constituent layers of a single bilayer have different chirp factors. The chirp factor considering an intermediate linear variation has been defined as,

$$f_j = \frac{d_{j,final}}{d_{j,initial}} \tag{4.5}$$

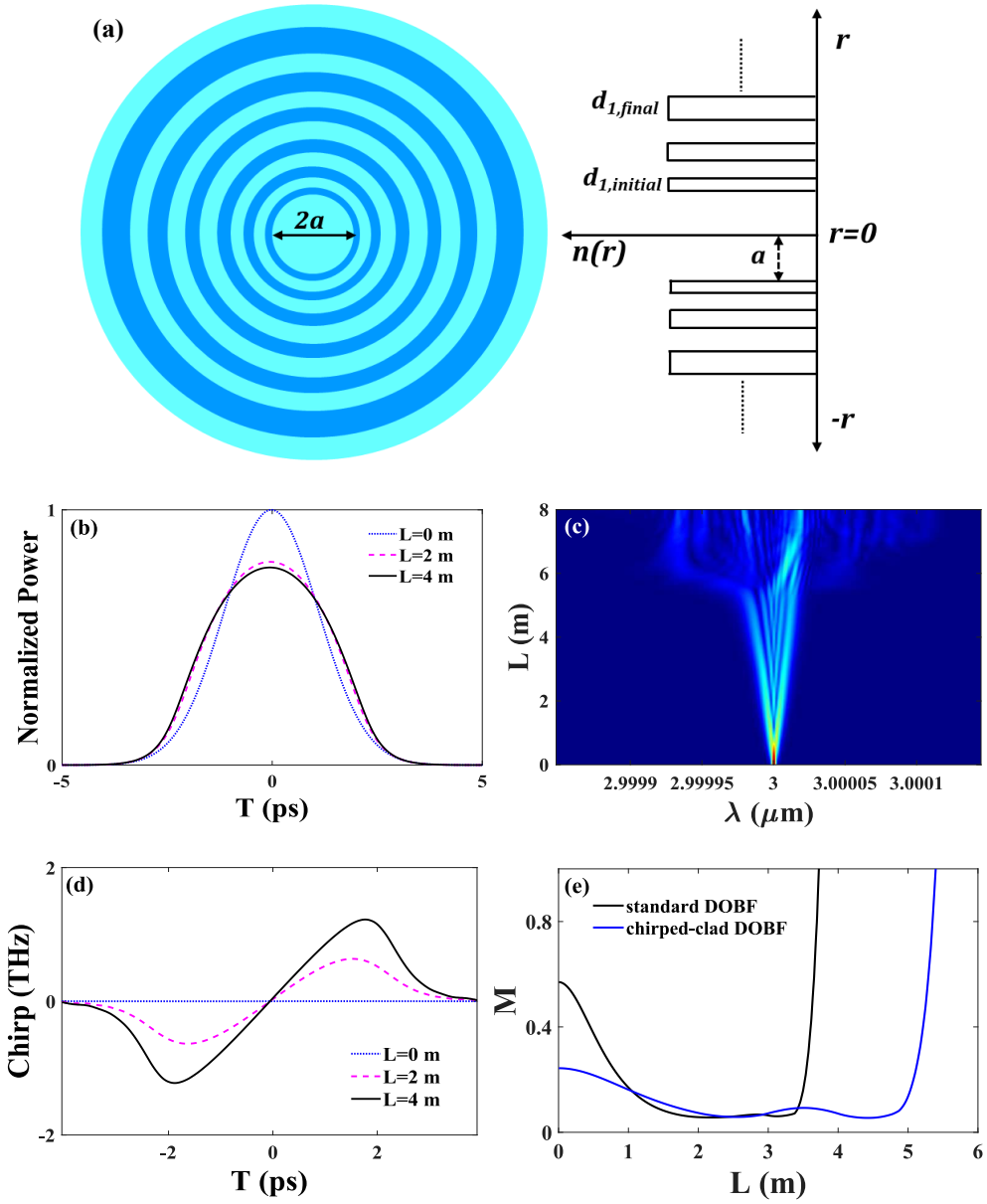

Figure 4.10: (a) The schematic representation of the chirped-clad Bragg cross-section along with the aperiodic refractive index profile, (b) the input and output pulse profiles through the chirped-clad DOBF in presence of TOD, (c) the corresponding spectral evolution, and (d) the chirp profile at various length of the chirped-clad DOBF, (e) the misfit parameter evolution in presence of TOD for a standard DOBF and a chirped-clad DOBF.

where $j = 1, 2$ for high and low index layers respectively. To estimate the fiber parameters and the losses for the fundamental mode, modal analysis have been carried out using TMM. The schematic of the chirped-clad transverse cross-section has been shown in figure 4.10(a) along with the linearly chirped refractive index profile. The specifications of the initial fiber cross-section are as follows: core radius $a = 4.5$ μm, $d_{1,initial} = 0.695$ μm, and $d_{2,initial} = 2.94$ μm. Here, the chirp factor for the high index layers f_1 has been varied from 0.9 to 1.5, and that for the low index layers f_2 has been varied from 0.95 to 1.05 over 6 bilayers. Such transverse chirping has resulted in a controlled dispersion profile with a very low confinement loss at 3.0 μm for the fundamental mode. It is to mention here that such transverse chirping allows less constraint on the choice of operating wavelength due to the overlap between the bandgaps corresponding to the innermost and the outermost bilayers, and thus it is convenient to choose the wavelength as per the requirement. With the chirped-clad Bragg cross-section, the Fiber I has been longitudinally down-tapered with a taper-ratio 0.85 over 2m. Similarly, the 1 m long section of the Fiber II segment, having its cross-section similar to the end cross-section of Fiber I, has been down-tapered with a taper-ratio 0.96 in a way such that it crosses the zero dispersion line. An alternate down and up-tapered arrangement of the Fiber II sections gives rise to the dispersion oscillating landscape.

A Gaussian pulse with peak power 150 W and FWHM 2.5 ps centered at 3.0 μm has been fed at the input end of the chirped-clad DOBF, and the propagation has been numerically studied by solving equation (4.4) with the estimated fiber parameters such as β_2, β_3 and γ as obtained from the modal analysis at various fiber lengths. A close investigation of pulse propagation reveals that parabolic pulses have been formed at nearly 1.5 m of the total fiber length with a misfit factor M = 0.025 and propagates self-similarly up to 4 m of the DOBF length. Figure 4.10(b) depicts the input Gaussian pulse along with the output parabolic pulse profiles at 2 m and 4 m, whereas figure 4.10(c) shows the evolution of the spectrum along the total fiber length. It has been explicit from the figures that a smooth parabolic pulse with FWHM ∼4 ps has been obtained up to the 4 m length of the chirped-clad DOBF. Moreover, a 3dB spectral broadening of ∼43 nm has been achieved at the end of 4 m fiber length. The corresponding chirp variation has been shown in figure 4.10(d) which is linear and symmetric without any hint of the presence of TOD. Moreover, the evolution of the misfit parameter M has also been depicted in figure 4.10(e) where the pulse evolution through the chirped-clad DOBF has been compared with that through the standard periodic-clad DOBF. From the misfit parameter evolution, the effect of transverse chirping on the reduction of TOD can be explicitly observed from the increased stable propagation length of the parabolic pulses in presence of TOD through the designed chirped-clad DOBF. However, the impact of the two-fold fiber design has limited prominence in this particular case due to the properties of chalcogenide glasses used for mid-IR range operation. For better understanding, the similar technique has been implemented for pulse propagation in the near-infrared range of wavelength where soft glasses with comparatively low dispersion and nonlinearity can be chosen for the fiber design as discussed in the next subsection.

4.5.2 Parabolic pulses in chirped-clad DOBF at near-IR

To implement the two-fold fiber engineering technique in near-IR range of wavelength, two commercially available soft glasses that exhibit excellent transmission properties around 1.0 μm wavelength has been chosen for the design of the chirped-clad dispersion oscillating Bragg fiber. The initial fiber cross-section has been optimized from the bandgap estimation and the optimized parameters are: core radius $a = 5.0$ μm, high index layer thickness $d_1 = 0.5$ μm, and low index layer thickness $d_2 = 4.9$ μm. With this initial specifications, the transverse chirping has been done by using the relation (4.5). The chirp factor for the high index layer f_1 has been linearly varied from 0.8 to 1.5 over 8 bilayers, and that for the low-index layer has been kept fixed i.e., $f_2 = 1$. Further, for the realization of the dispersion oscillation landscape the two fiber segments, namely

Fiber I and Fiber II has been designed with the chirped-clad initial cross-section. Here also, Fiber I has been a 2 m long segment with a taper-ratio 0.95 providing the decreasing dispersion profile for parabolic pulse formation, whereas Fiber II has been down-tapered with a ratio 0.96 over 1 m which has then been clubbed with other identical pieces of Fiber II in order to achieve the varying dispersion profile. The estimation of fiber parameters such as β_2, β_3, and γ has been done by the modal analysis of the chirped-clad fiber cross-section at various lengths of the tapered fiber and further interpolation of the estimated data. The total length of the chirped-clad DOBF has been 8 m.

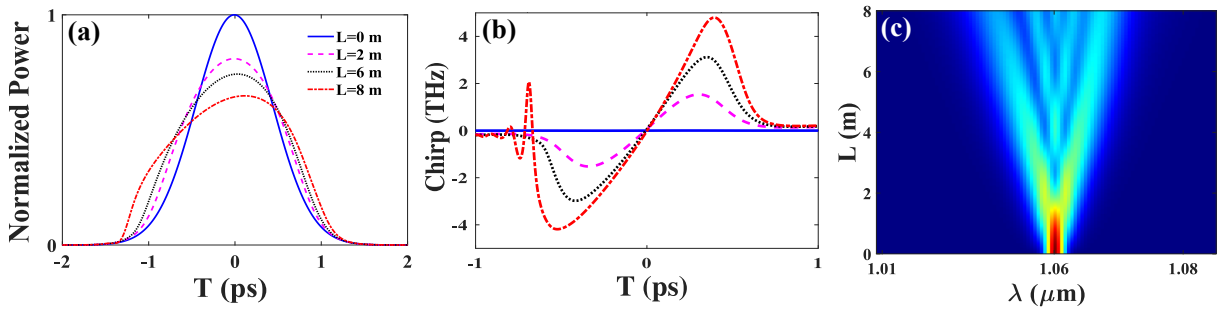

Figure 4.11: (a) The input and output pulse profiles at various fiber lengths in presence of TOD, and (b) the corresponding chirp variation, (c) the spectral evolution through the chirped-clad DOBF at 1.06 μm.

The impact of transverse chirping on the reduction of TOD effect has been investigated by launching a Gaussian pulse with 0.8 ps FWHM and 3.7 kW peak power centered at 1.06 μm at the input end of the designed chirped-clad DOBF. The pulse propagation has been studied by solving equation (4.4). A comparatively stable parabolic pulse with its characteristic linear chirp across the entire width of the pulse has been observed up to 8 m length of the chirped-clad DOBF. Figure 4.11(a) depicts the evolution of the input Gaussian to a parabolic form at various fiber lengths. An asymmetry in the temporal pulse profile at the end of the fiber can be observed which is a clear indication of the presence of TOD effect. However, the almost distortion free time-domain pulse profile along the entire fiber length has explicitly indicated the suppression of TOD effect which is the best consequence of transverse chirping in the dispersion oscillating landscape. The output chirp has been shown in figure 4.11(b) which also shows a linear variation with a slight asymmetry due to the presence of TOD. The spectral evolution has been depicted in figure 4.11(c) which again proves the stability of pulse propagation as the evolution is smooth and almost symmetric throughout the fiber length.

4.6 Conclusions

In summary, formation and stable propagation of high power ultrashort parabolic pulses has been demonstrated in a highly dispersive and highly nonlinear environment preceding the wave-breaking regime of propagation. Parabolic pulses with linear frequency chirp are observed to be able to carry such high power. However, fiber-based formation of robust parabolic pulses in the mid-IR range of wavelength poses certain challenges. The foremost challenge is to deliver stable parabolic pulses through passive nonlinear reshaping, since operating in the mid-IR range of wavelength compels to use chalcogenide glasses for fibers which are highly dispersive as well as highly nonlinear compared to silica or other soft glasses. It has already been observed that high nonlinearity triggers the reshaping process much faster followed by optical wave-breaking due to higher dispersion preceding the wave-breaking length, and the parabolic pulses formed in this way are mere transient state of propagation. Thus, it has been of utmost importance to control the fiber

dispersion to avoid the transient state of propagation and to enter the robust state of parabolic pulse. Towards this, a fiber design scheme has been proposed which implements a varying dispersion profile along the fiber length with a close-to-zero average GVD value. A Bragg fiber cross-section has been optimized to operate at 2.8 μm wavelength which finds a lot of bio-medical applications. Further, two fiber segments has been designed - one 2 m long dispersion decreasing segment, namely Fiber I, for the formation of parabolic pulse; the other one, namely Fiber II, is a total 6 m long multi-segment fiber section comprising of six 1 m long tapered sections alternately joined to form a oscillating dispersion profile. Notable, in Fiber II both the normal and the anomalous dispersion regimes have been covered with a global small positive average GVD. A high power Gaussian pulse have been allowed to propagate through the designed DOBF, and a stable distortion free parabolic pulse with linear chirp has been obtained at the end of the 8 m long fiber. The breather like evolution of the formed parabolic pulse through the Fiber II indicates a better dispersion control unlike any conventional DDF. To appreciate the impact of oscillating dispersion profile, two and three consecutive pulses with high repetition rate ($\sim$167 GHz) has been allowed to evolve through the DOBF which results in stable output parabolic pulses. This has happened due to the controlled dispersion in Fiber II resulting in a very little amount of dispersion-induced pulse broadening. Moreover, SPM and intrapulse Raman effects together have been taken into account to explore the spectral broadening through such DOBF. As a result, a 1.5 ps Gaussian pulse reshapes into a parabolic pulse due to interplay of dispersion and nonlinearity and maintain this parabolic shape over 8 m of the fiber length with a mid-IR spectral broadening up to 465 nm at 20dB point. Such results have also been compared with that obtained from a DDF. Furthermore, spectral and temporal changes beyond wave-breaking have also been investigated. Such findings would eventually be applicable to studies that require high intensity spectra over a wide band along with well-defined temporal pulse profile. Finally, the effect of third order dispersion has been included to the pulse propagation, since there are several zero crossings in the DOBF which eventually make the inclusion of TOD effect crucial. As anticipated, the presence of TOD readily distorts the parabolic pulses within a very short range after their formation. To suppress the detrimental TOD effect, a transverse chirping in the fiber cladding region has been implemented along with the longitudinal oscillating dispersion profile. Such two-fold fiber engineering has stabilized the parabolic pulse up to 4 m of the chirped-clad DOBF length at mid-IR. To further appreciate the impact of transverse chirping, a chirped-clad DOBF has been designed at near-IR wavelength using a pair of soft glasses, which has allowed a stable distortion free transmission of high power ultrashort parabolic pulse up to 8 m. A judicious choice of materials and fiber parameters would eventually provide robust high power pulse delivery through such dispersion oscillating landscape.

4.6.1 Applications

Short-length fibers delivering stable pulses with moderately high power (in the range of several hundred watts to few kilo-Watts) are essentially required in applications like fiber-based mid-IR bio-medical imaging devices, laser-based surgery such as tissue ablation, and dental surgery, precision machining, pulse-preserving supercontinuum generation and so on. The proposed dispersion oscillating fibers are very much suitable not only for stable high power beam delivery, but also in various spectroscopic measurements owing to the wide continuous spectrum supported by such fibers.

4.6.2 Impact statement

The dispersion oscillating fibers proposed in this chapter are one of a kind novel fiber geometry that readily exhibit excellent stability in the formation of self-similar parabolic pulses withstanding a large amount of dispersion and nonlinearity. The implemented rapidly varying dispersion profile with nearly-zero average dispersion has been the first ever report by exploiting

the fiber tapering process which in turn provides ample degree-of-freedom for further engineering of the fiber geometry, and to play with the fiber parameters as required. Moreover, such varying dispersion profile sync well with any further cross-sectional variation keeping the output pulse forms unperturbed, which readily adds another degree-of-freedom in fiber engineering process. Thus, such dispersion oscillating landscape readily leads to an intriguing area of study on unconventional spatio-temporal dynamics of light in presence of varying dispersion and nonlinear properties for specialty applications.

Moreover, the outcome of this research eventually propel the development of all-fiber based photonic devices, specifically for mid-IR based bio-medical equipment with enhanced performance. The temporal stability of high power pulses would be beneficial for bio-medical surgeries, whereas the spectral broadening would facilitate the implementation of fiber-based high-resolution imaging devices. In addition, development of high power parabolic pulsed lasers through dispersion oscillating fiber can be a broad domain of study for strategic and industrial purposes.